9th Internat. Symp. on Cyclodextrins, Santiago de Compostela, **1998**
(Eds.: J.J. Torres Labandeira, J.L. Vila Jato),
Kluwer Acad. Publ., Dordrecht, NL, **1999**, pp. 41-48.

a-CYCLOALTRIN: CONFORMATION AND PROPERTIES IN THE SOLID-STATE AND AQUEOUS SOLUTION[1]

S. IMMEL, G. E. SCHMITT, AND F. W. LICHTENTHALER

Institute of Organic Chemistry, Darmstadt University of Technology, D-64287 Darmstadt, Germany

Abstract. Analysis of the conformational properties of α-cycloaltrin (α-CA) in aqueous solution by 800 MHz ^{1}H, 200 MHz ^{13}C NMR, and molecular dynamics (MD) simulations points towards a complex equilibrium of $^{4}C_1 \rightleftharpoons {}^{O}S_2 \rightleftharpoons {}^{1}C_4$ altropyranose units. Although the $^{3}J_{H\text{-}H}$ coupling constants do not reveal a preference for the alternating $^{4}C_1$ / $^{1}C_4$ or the *all*-$^{O}S_2$ conformation of α-CA, low-temperature ^{13}C NMR line-broadening indicates at least two different conformations of the altrose residues. Both α-CA geometries are stable during 600 ps MD simulations without conformational transitions, but constrained MDs forcing one altropyranose unit to vary along the $^{4}C_1 \rightarrow {}^{O}S_2 \rightarrow {}^{1}C_4$ reaction coordinate indicates cooperative conformational transitions $^{1}C_4 \rightarrow {}^{O}S_2 \rightleftharpoons {}^{3,O}B$ of neighboring units and statistical scrambling of the pyranose geometries in the macrocycle. In particular, the *all*-$^{O}S_2$ conformation of α-CA features a central cavity capable to form inclusion complexes, whereas alternate forms may have surface indentations only.

1. Introduction

In the course of our molecular modeling studies on the hydrophobic characteristics of the cyclodextrins[2], we have pointed out that inversion of the configuration at C-2 (→ D-mannose) leads to a significantly enhanced lipophilicity of the central cavities in the corresponding cyclomannins[3]. The opposite is to be expected for the C-3 epimers of the cyclodextrins, i.e. the as yet unknown cycloallins, although the axial 3-OH groups, now reaching into the cavities, are likely to introduce additional strain on the macrocycles and, hence, distortion. Even more intriguing are the synthetically readily accessible cycloaltrins[4,5], since two axial hydroxyl groups not only impose strain on the macrorings, but also render the monosaccharide units with considerable flexibility.

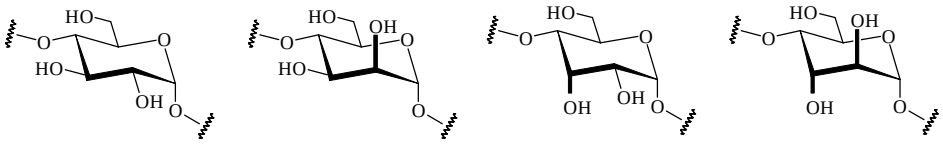

cyclodextrins **cyclomannins** **cycloallins** **cycloaltrins**

The very small energy difference for the $^{4}C_1$ (shown above) and $^{1}C_4$ conformation of α-D-altropyranose – computed values vary from +0.8[6] to -1.5 kJ/mol[7] – leads to a unique solid-state structure of α-cycloaltrin (**1**)[5], in which nearly perfect $^{4}C_1$ and $^{1}C_4$ chairs are arranged in an alternating sequence in a C_3 symmetrical conformation (cf. Fig. 1). Although this geometry lacks a "through-going" cavity, HTA calculations of **1** in vacuum yield an *all*-skew (twist-boat) $^{O}S_2$-geometry as the global energy-minimum structure, which features a cavity[5,8].

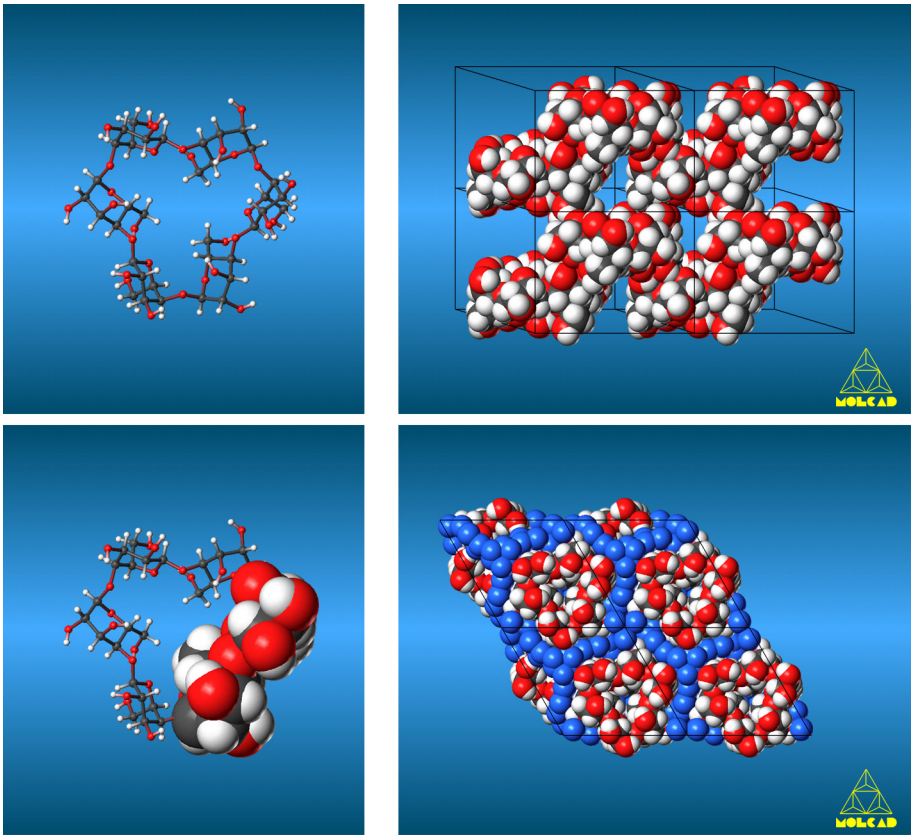

Figure 1. The α-cycloaltrin (**1**) solid-state structure features a rather compact conformation of 3-fold rotational symmetry with an alternating sequence of $^{4}C_{1}$ and $^{1}C_{4}$ altropyranose chairs (upper left); the constituent $^{4}C_{1}/^{1}C_{4}$-disaccharide units — of which one is represented in space filling form (lower right) — are of banana-type shape. In the crystal lattice, the molecules are stacked in transposed layers on top of each other (upper right side-view, water molecules were left of for clarity). The crystals are heavily hydrated, and each of the α-CA molecules is embedded into a matrix of 21 water molecules (lower right, top view).

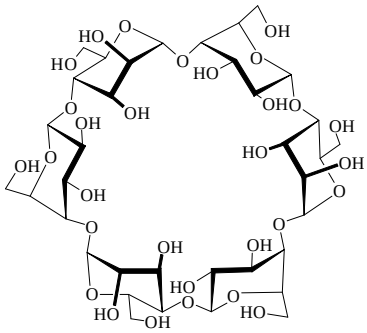

$^{4}C_{1}/^{1}C_{4}$ conformation (solid-state, **1a**)

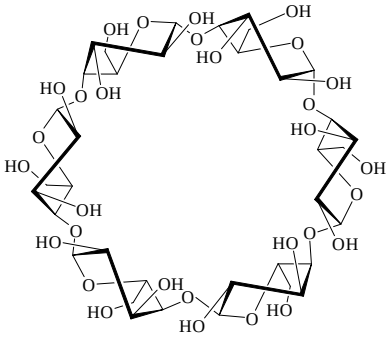

all-$^{O}S_{2}$ conformation (calculated, **1b**)

α-cycloaltrin (**1**)

To get some insight into the conformation of α-cycloaltrin in aqueous solution we performed molecular dynamic simulations and temperature dependent NMR studies.

2. Methods

Temperature dependent ^{1}H (800 MHz) and ^{13}C (200 MHz) spectra were recorded at the "Large Scale Facility for Biomolecular NMR" in Frankfurt[9].

HTA[5] and the MD calculations were carried out using the CHARMM[10] force-field[11], comprising application of periodic boundaries (truncated octahedron filled with 606 (**1a**) and 611 (**1b**) water molecules, respectively), isothermal (T = 300 K), and isobaric conditions (p = 1 bar) during a simulation time of 600 ps (timestep 1 fs); analysis of the MD trajectories were accomplished with external computer programs[12].

3. Results and Discussion

Temperature Dependent NMR Analysis. — High-resolution ^{1}H and ^{13}C NMR spectroscopy of **1** (D_2O, 30 °C) displays only one set of signals for the six altropyranoses, indicating that, alternatively, fast conformational averaging between different pyranose ring forms takes place, or that – in contrast to the solid-state – a unique altrose geometry prevails in solution.

The ^{1}H NMR coupling constants are consistent with either scenario: as indicated in Table 1, the experimental values agree with an average between the $^{4}C_1$ and $^{1}C_4$ forms (geometry **1a**), but correlate also surprisingly well with the values calculated for the *all*-$^{O}S_2$ form **1b**.

Table 1. Comparison of the altropyranoid ring ^{1}H-^{1}H-coupling constants calculated for the $^{4}C_1$, $^{1}C_4$, and *all*-$^{O}S_2$ (skew) forms of α-cycloaltrin with those found (800 MHz, D_2O, 30 °C).

$^{3}J_{HH}$ [Hz][a]	$^{4}C_1$[b]	$^{1}C_4$[b]	$^{O}S_2$[c]	found	calc.[d]
$J_{1,2}$	2.2	8.0	4.0	4.73	4.9
$J_{2,3}$	2.7	10.2	10.2	8.19	8.3
$J_{3,4}$	3.4	2.4	4.5	3.71	3.5
$J_{4,5}$	9.7	1.4	6.4	5.32	5.5

[a] Calculation based on the generalized Haasnoot-equation[13]. [b] calc. for the pyranose conformations in **1a**. [c] calc. for **1b**. [d] least-squares fit for 26% $^{4}C_1$, 34% $^{1}C_4$, and 40% $^{O}S_2$ (cf. text)[14].

The presence of conformational equilibria in aqueous solutions of **1** is indicated by the temperature dependency of its ^{1}H NMR data: the value of $J_{2,3}$ decreases from 8.2 Hz at 30 °C to 7.6 and 7.1 Hz at 20 and 4 °C, respectively, thereby narrowing the well separated signal for 3-H. Although the decreasing value of $J_{2,3}$ with decreasing temperature points towards the $^{4}C_1$ altrose conformation to be the most stable form in the $^{4}C_1 \rightleftharpoons {}^{O}S_2 \rightleftharpoons {}^{1}C_4$ pyranose pseudorotational itinerary, as this form shows the lowest calculated coupling constant (cf. Table 1), the best fit of calculated vs. measured coupling constants was achieved for an approx. 1 : 1 : 1 mixture of $^{4}C_1$, $^{O}S_2$, and $^{1}C_4$ forms[14] (cf. Table 1).

More profound effects are observed for the ^{13}C signals for C-4 and C-5, which are substantially broadened upon lowering the temperature from 30 to 4 °C (cf. Fig. 2),

providing further evidence for a dynamic equilibrium of various altrose geometries which starts to "freeze-out" at 4 °C.

However, the NMR data do neither provide a picture how different conformations are accessible within the "strait-jacket" of the α-CA macrocycle, nor do they answer the question how conformational transitions occur in **1** (e.g. **1a** ⇌ **1b**).

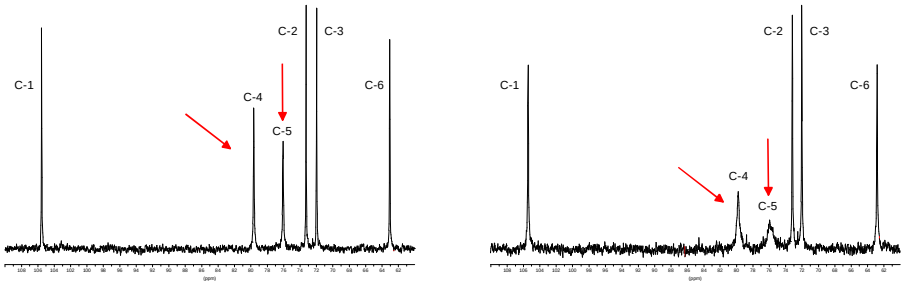

Figure 2. ^{13}C NMR spectra (200 MHz) of α-cycloaltrin (**1**) in D_20 at 32 °C (left) and 4 °C (right). As indicated by the arrows, the signals of C-4 and C-5 undergo significant broadening at the lower temperature.

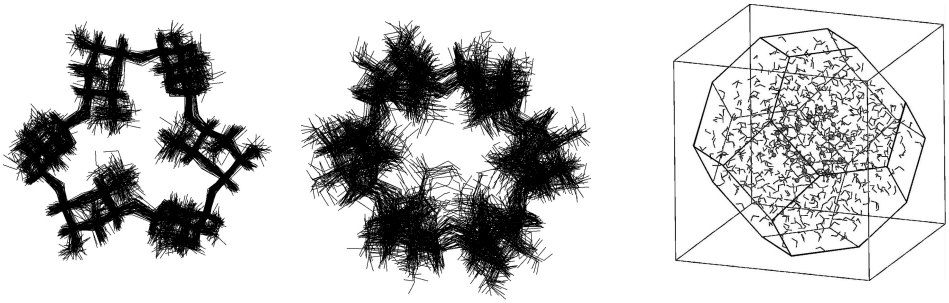

$^4C_1$ / $^1C_4$ conformation **1a** *all*- $^OS_2$ conformation **1b** MD simulation box

Figure 3. Superimpositions of 60 α-cycloaltrin snapshot-geometries taken in 10 ps intervals from MD simulations of **1a** (left) and **1b** (center) display the flexibility of the macrocycles, although the pyranose ring conformations are rather rigid. On the right, a typical MD simulation box (truncated octahedron) filled with water is depicted.

Figure 4 (opposite page). Constrained MD simulations of α-CA display a conformational transition of the central $^4C_1$ altropyranose (gray shaded unit **B**) of a $^1C_4$-$^4C_1$-$^1C_4$-fragment (units **A**-**B**-**C**) in the macrocycle: as **B** is driven along the $^4C_1 \rightarrow {}^{3,O}B$ / $^OS_2 \rightarrow {}^1C_4$ reaction coordinate (formulas, left column), the conformation of the neighboring residue **A** varies very little with slight distortions $^1C_4 \rightarrow {}^3H_2$ only, but the altrose unit **C** cooperatively flips into the $^{3,O}B \rightleftharpoons {}^OS_2$ geometry (zoomed structures on the right). The unperturbed and cooperative conformational transitions of adjacent pyranose units point towards complex dynamic processes, in the course of which the altrose residues cannot be considered independent; each conformational change induces new strains in neighboring units (all α-CA snap-shot structures were taken from a 1300 ps MD perturbation, and constraints were applied to unit **B** only; for details see text).

unit **B**:

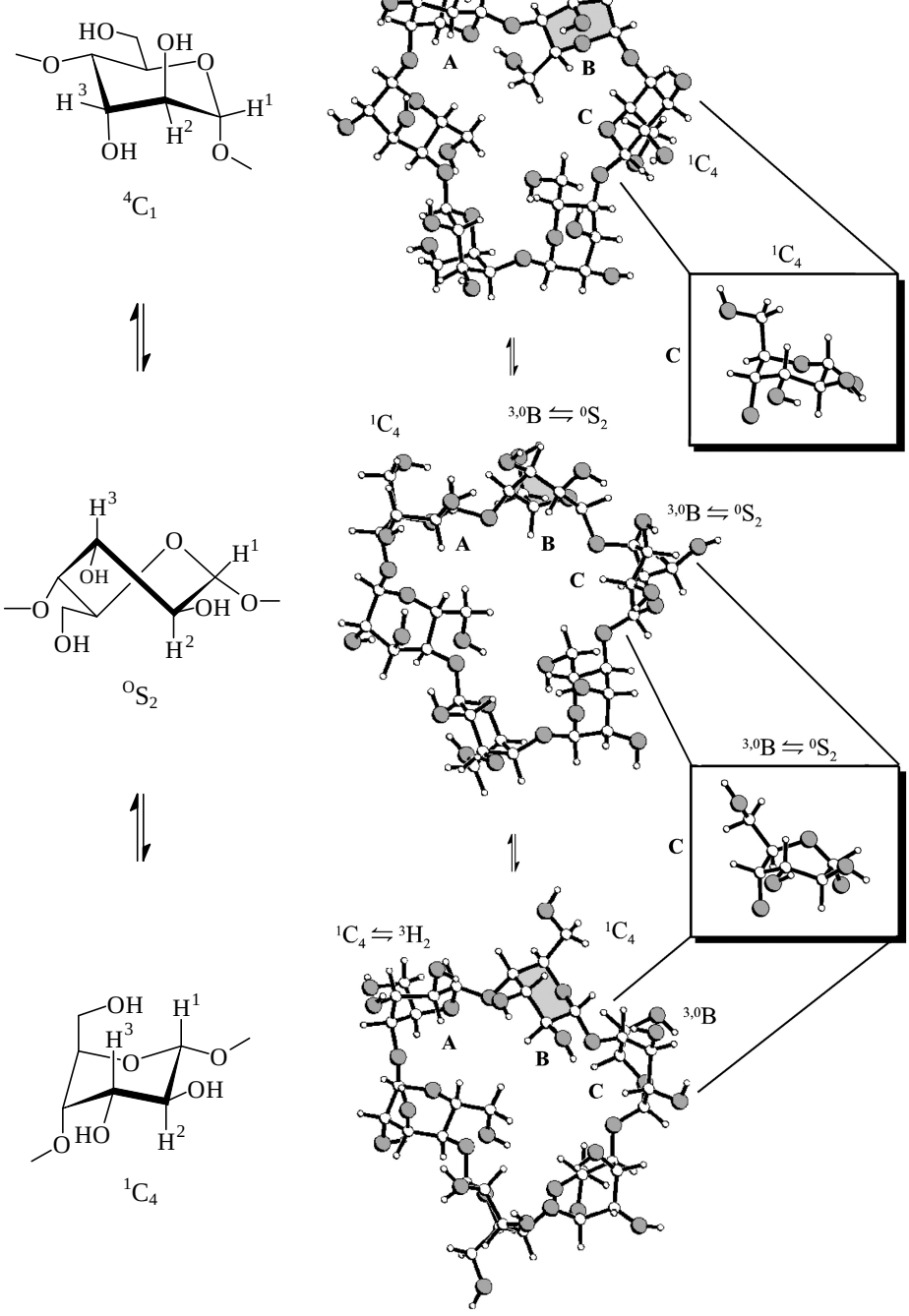
$^4C_1$
$^1C_4$
$^0S_2$
$^1C_4$
$^3B \rightleftharpoons {}^0S_2$
$^1C_4 \rightleftharpoons {}^3H_2$
^3B
A
B
C

*Molecular Dynamics Simulations of **1***. — For both α-CA forms **1a** and **1b**[8] MD simulations with explicit incorporation of the (aqueous) solvent were performed. Although the macrocycles display a considerable degree of flexibility, no significant conformational transitions for the pyranose units were observed within a time frame of 600 ps (Fig. 3). From these calculations, the solute hydration shells can be readily identified, with an average of 30.6 ± 2.7 and 39.6 ± 3.4 water molecules being hydrogen bonded to **1a** and **1b**, respectively. Obviously, any change of the pyranose conformations entails substantial rearrangements in the tightly bound first hydration shell, rendering these processes too slow to be observable during standard MD simulations.

The effects on the macrocycle of changing one altrose unit in **1a** along the $^4C_1 \rightarrow {}^OS_2 \rightarrow {}^1C_4$ pathway can be monitored within a reasonable nanosecond time frame by using constrained MD techniques: two pyranose ring torsion angles O_5-C_1-C_2-C_3 and C_3-C_4-C_5-O_5 of one altrose unit are restrained in such a way, that the $^4C_1$ conformation is forced to vary in the desired direction (Fig. 4, gray shaded altrose residue **B**). As this ring flip is artificially induced, the neighboring unconstrained monosaccharide units are subject to considerable intrinsic strain in the macro-ring: as one unit remains only slightly distorted towards $^1C_4 \rightarrow {}^3H_2$ (unit **A** in Fig. 4), the second adjoining residue (**C**) displays a full transition along $^1C_4 \rightarrow {}^OS_2 \rightleftharpoons {}^{3,O}B$. As this ring-flip was not induced by additionally applied MD potentials, it reveals the way conformational changes occur within α-CA (**1**). Flexure of the altrose chair geometries must involve $^OS_2$ forms, cooperatively affecting neighboring units to also flip into this intermediate as these are tied up in a macrocyclic "strait-jacket".

The consecutive "rolling around" of geometry changes in the conceivably elliptically distorted macrocycle leads to a statistical scrambling of $^4C_1$, $^1C_4$, and $^OS_2$ forms in **1** in aqueous solution, and the NMR data provide an averaged picture thereof. As the two forms **1a** and **1b** are to be considered as the limiting structures of a complex equilibrium only, the inclusion complex formation capabilities of α-CA (**1**) must be closely correlated to its solution conformations, of which only the *all*-$^OS_2$ form **1a** features a sizable "through-going" cavity with which to incorporate potential guest molecules.

*Molecular Lipophilicity Patterns of **1***. — The MOLCAD-program[15] mediated color-coded projection[16] of the molecular lipophilicity patterns (MLPs)[17] onto the surfaces[18] of the solid-state conformation **1a** and the HTA-derived energy-minimum *all*-$^OS_2$ form **1b** (cf. Fig. 5) allow a first assessment of the inclusion complex formation capabilities of α-cycloaltrin: in both forms **1a** and **1b** a distinct front/back differentiation of hydrophobic and hydrophilic surface regions is manifested in Fig. 5. In analogy to the cyclodextrins[2], the side of the disk- (**1a**) or torus-shaped (**1b**) macrocycle carrying the secondary 2-OH and 3-OH groups turns out to be the most hydrophilic part of the molecule, whereas the back is significantly more hydrophobic due to its association with the primary 6-CH_2OH groups. Although **1a** lacks a central "through-going" cavity, it features a hydrophilic surface indentation. As displayed in the side-view projections of the MLPs, the outer core of **1a** is made up by irregularly distributed hydrophilic and hydrophobic regions (Fig. 5, top right). This is contrasted by the cyclodextrin-like torus-shaped from **1b**, in which the corresponding surface qualities display a more uniform pattern (Fig. 5, bottom): the most hydrophobic surface areas extend from the 6-OH side

well into the cavity. However, in relation to the cyclodextrins the *all*-$^{O}S_2$ form is characterized by an inverse tilt of the pyranose units in the macrocycle. Unlike α-CD[2], the cycloaltrin cavity is narrow at its hydrophilic end and wider at the hydrophobic surface. As the form **1b** of α-CA is the first cyclooligosaccharide of *"inverse conicity"* with an extended hydrophobic cavity, we expect — if this conformation is adopted — a high potential of this compound to form inclusion complexes in solution and the solid-state.

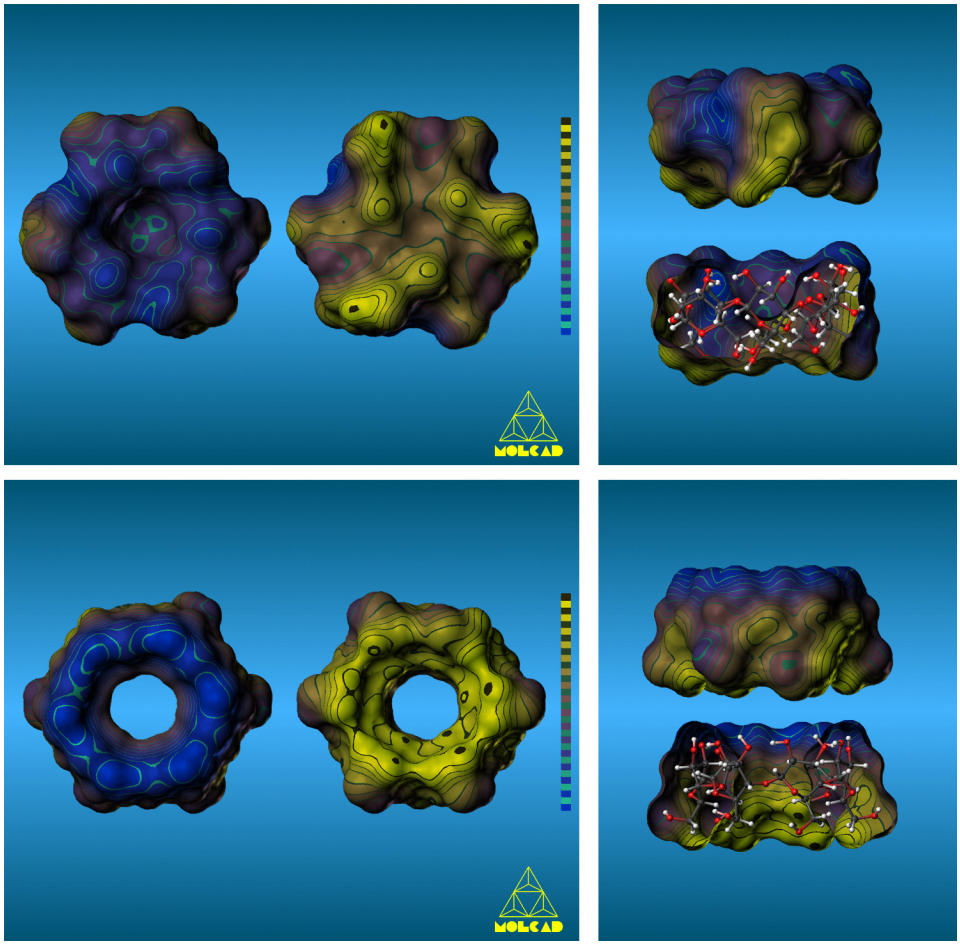

Figure 5. Molecular lipophilicity patterns (MLPs) of α-CA (**1**) projected onto the contact surfaces of the solid-state conformation (**1a**, top) and the *all*-$^{O}S_2$ form (**1b**, bottom). The color-code applied ranges from dark blue for the most hydrophilic surface areas to full yellow corresponding to the most hydrophobic regions. On the left each, the macrocycles are viewed from both sides perpendicular to the mean ring plane, exposing either the pronouncedly hydrophilic (blue) 2-OH/3-OH side of the torus or the opposite, hydrophobic rim made up by the primary 6-CH_2OH hydroxyls. The right graphics display the corresponding side-views in closed and bisected form each; the 2-OH and 3-OH groups are directed upwards, whereas the 6-OH point downwards.

References

[1] 'Molecular Modeling of Saccharides', Part 18. — Part 17: Gohlke, H.G., Immel, S., Lichtenthaler, F.W., and Schmitt, G.E. (1998). Molecular geometries of furanoid β(1→3)- and β(1→6)-linked cyclogalactins, in Torres Labandeira, J.J. (Ed.), *Proceedings 9th Internat. Symp. on Cyclodextrins*, Kluwer Acad. Publ., Dordrecht, NL.

[2] Lichtenthaler, F.W., and Immel, S. (1996). On the hydrophobic characteristics of cyclodextrins: computer-aided visualization of molecular lipophilicity patterns. *Liebigs Ann. Chem.*, 27-37.

[3] Lichtenthaler, F.W., and Immel, S. (1994). Cyclodextrins, cyclomannins, and cyclogalactins with five and six (1→4)-linked sugar units: a comparative assessment of their conformations and hydrophobicity potential profiles. *Tetrahedron: Asymmetry*, *5*, 2045-2060. — Lichtenthaler, F.W., and Immel, S. (1996). The lipophilicity patterns of cyclodextrins and non-glucose cyclooligosaccharides. *J. Inclusion Phenom. Mol. Recognit. Chem.*, *25*, 3-16.

[4] Fujita, K., Shimada, H., Ohta, K., Nogami, Y., Nasu, K., and Koga, T. (1995). β-Cycloaltrin: a cyclooligosaccharide consisting of seven α-(1→4)-linked altropyranoses. *Angew. Chem. Int. Ed. Engl.*, *34*, 1621-1622. - Nogami, Y., Fujita, K., Ohta, K., Nasu, K., Shimada, H., Shinohara, C., and Koga, T. (1996). A new synthetic strategy of cyclooligosaccharides: cyclodextrin-derived cycloaltrins made up from α-(1→4)-linked altropyranoses. *J. Inclusion Phenom. Mol. Recognit. Chem.*, *25*, 57-60.

[5] Nogami, Y., Nasu, K., Koga, T., Ohta, K., Fujita, K., Immel, S., Lindner, H.J., Schmitt, G.E., and Lichtenthaler, F.W. (1997). Synthesis, structure, and conformational features of α-cycloaltrin: a cyclooligosaccharide with alternating $^4C_1/^1C_4$ pyranoid chairs. *Angew. Chem. Int. Ed. Engl.*, *36*, 1899-1902.

[6] Angyal, S.J. (1968). The conformations and α-β-ratios of aldopyranoses in aqueous solution. *Aust. J. Chem.*, *21*, 2737-2746.

[7] Dowd, M.K., French, A.D., and Reilly, P.J. (1994). Modeling of aldopyranosyl ring puckering with MM3(92). *Carbohydr. Res.*, *264*, 1-19.

[8] The 3D-structures can be viewed at "http://caramel.oc.chemie.tu-darmstadt.de/immel/3Dstructures.html", MOLCAD graphics are available at "http://caramel.oc.chemie.tu-darmstadt.de/immel/molcad/gallery.html".

[9] We are most grateful to Prof. Dr. C. Griesinger and Dr. H. Schwalbe, for kindly determining the 800 (^{1}H) and 200 (^{13}C) MHz NMR data at the 'Large Scale Facility for Biomolecular NMR' of Frankfurt University.

[10] Brooks, B.R., Bruccoleri, R.E., Olafson, B.D., States, D.J., Swaminathan, S., and Karplus, M. (1983). CHARMM: a program for macromolecular energy, minimization, and dynamics calculations. *J. Comp. Chem.*, *4*, 187-217.

[11] Reiling, S., Schlenkrich, M., and Brickmann, J. (1996). Force field parameters for carbohydrates. *J. Comput. Chem.*, *17*, 450-468.

[12] Immel, S. (1997). *MolArch+ - MOLecular ARCHitecture Modeling Program*, Darmstadt University of Technology.

[13] Haasnoot, C.A.G., De Leeuw, F.A.A.M., and Altona, C. (1980). The relationship between proton-proton NMR coupling constants and substituent electronegativities. *Tetrahedron*, *36*, 2783-2792.

[14] Least-squares fitting of the *J* values for three conformations $^4C_1$, $^1C_4$, and $^OS_2$ was achieved with a root-mean-square deviations of $\sigma_J = 0.3$ Hz, whereas a two-state model $^4C_1 \rightleftharpoons {}^1C_4$ yielded $\sigma_J = 1.8$ Hz only.

[15] Brickmann, J. (1997). *MOLCAD - MOLecular Computer Aided Design*, Darmstadt University of Technology. — Brickmann, J. (1992). Molecular graphics: how to see a molecular scenario with the eyes of a molecule. *J. Chim. Phys.*, *89*, 1709-1721.

[16] Teschner, M., Henn, C., Vollhardt, H., Reiling, S., and Brickmann, J. (1994). Texture mapping: a new tool for molecular graphics. *J. Mol. Graphics*, *12*, 98-105.

[17] Heiden, W., Moeckel, G., and Brickmann, J. (1993). A new approach to analysis and display of local lipophilicity/hydrophilicity mapped on molecular surfaces. *J. Comput.-Aided Mol. Des.*, *7*, 503-514.

[18] Connolly, M.L. (1983). Analytical molecular surface calculation. *J. Appl. Cryst.*, *16*, 548-558.